HHS Public Access

Author manuscript

J Am Chem Soc. Author manuscript; available in PMC 2023 January 12.

Published in final edited form as:

J Am Chem Soc. 2022 January 12; 144(1): 282–287. doi:10.1021/jacs.1c09581.

Temperature Cycling Enables Efficient ^{13}C SABRE-SHEATH Hyperpolarization and Imaging of [1-^{13}C]-Pyruvate

Patrick TomHon[a,*], **Mustapha Abdulmojeed**[a], **Isaiah Adelabu**[b], **Shiraz Nantogma**[b], **Mohammad Shah Hafez Kabir**[b], **Sören Lehmkuhl**[a], **Eduard Y. Chekmenev**[b,c,d], **Thomas Theis**[a,e,f,*]

[a]Department of Chemistry, North Carolina State University, Raleigh, NC 27606, United States

[b]Department of Chemistry, Wayne State University, Detroit, MI 48202, United States

[c]Integrative Biosciences (Ibio), Wayne State University, Karmanos Cancer Institute (KCI), Detroit, MI 48202, United States

[d]Russian Academy of Sciences, Leninskiy Prospekt 14, 119991 Moscow, Russia

[e]Joint Department of Biomedical Engineering, University of North Carolina, Chapel Hill and North Carolina State University, Raleigh, North Carolina 27606, United States

[f]Department of Physics, North Carolina State University, Raleigh, NC 27606, United States

Abstract

Molecular metabolic imaging in humans is dominated by positron emission tomography (PET). An emerging non-ionizing alternative is hyperpolarized MRI of ^{13}C-pyruvate, which is innocuous and has a central role in metabolism. However, similar to PET, hyperpolarized MRI with dissolution dynamic nuclear polarization (d-DNP) is complex, costly and requires significant infrastructure. In contrast, Signal Amplification By Reversible Exchange (SABRE) is a fast, cheap, and scalable hyperpolarization technique. SABRE in SHield Enables Alignment Transfer to Heteronuclei (SABRE-SHEATH) can transfer polarization from parahydrogen to ^{13}C in pyruvate, however, polarization levels remained low relative to DNP (1.7% with SABRE-SHEATH vs.

[*]**Corresponding Authors** Patrick TomHon – *Department of Chemistry, North Carolina State University, Raleigh, North Carolina 27695, United States,* pmtomhon@ncsu.edu; Thomas Theis – *Department of Chemistry, North Carolina State University, Raleigh, North Carolina 27695, United States; Joint Department of Biomedical Engineering, University of North Carolina, Chapel Hill and North Carolina State University, Raleigh, North Carolina 27606, United States; Department of Physics, North Carolina State University, Raleigh, North Carolina 27695, United States,* ttheis@ncsu.edu.
Mustapha Abdulmojeed – *Department of Chemistry, North Carolina State University, Raleigh, North Carolina 27695, United States*
Isaiah Adelabu – *Department of Chemistry, Wayne State University, Detroit, Michigan 48202, United States*
Shiraz Nantogma – *Department of Chemistry, Wayne State University, Detroit, Michigan 48202, United States*
Mohammad Shah Hafez Kabir – *Department of Chemistry, Wayne State University, Detroit, Michigan 48202, United States*
Sören Lehmkuhl – *Department of Chemistry, North Carolina State University, Raleigh, North Carolina 27695, United States*
Eduard Y. Chekmenev – *Department of Chemistry, Wayne State University, Detroit, Michigan 48202, United States; Integrative Biosciences (Ibio), Wayne State University, Detroit, MI, 48202, United States; Karmanos Cancer Institute (KCI), Wayne State University, Detroit, MI, 48202, United States; Russian Academy of Sciences, Leninsky Prospekt 14, 119991 Moscow, Russia*

ASSOCIATED CONTENT

The Supporting Information is available free of charge at http://pubs.acs.org.
Additional figures and results as discussed in the text.

Thomas Theis holds stock in Vizma Life Sciences LLC (VLS) and is President of VLS. VLS is developing products related to the research being reported. The terms of this arrangement have been reviewed and approved by NC State University in accordance with its policy on objectivity in research. The authors have filed a provisional patent application through NC State University with the USPTO regarding this work (Application# 63/203,591). EYC discloses a stake of ownership in XeUS Technologies, LTD.

≈60% with DNP). Here we introduce a temperature cycling method for SABRE-SHEATH that enables >10% polarization on [1-^{13}C]-pyruvate, sufficient for successful *in vivo* experiments. First, at lower temperatures, ≈20% polarization is accumulated on SABRE-catalyst bound pyruvate, which is released into free pyruvate at elevated temperatures. A kinetic model of differential equations is developed that explains this effect and characterizes critical relaxation and build-up parameters. With the large polarization, we demonstrate the first ^{13}C pyruvate images with a cryogen-free MRI system operated at 1.5 T, illustrating that inexpensive hyperpolarization methods can be combined with low-cost MRI systems to obtain a broadly available, yet highly sensitive metabolic imaging platform.

Graphical Abstract

New techniques and fundamental insights in hyperpolarization chemistry provide high nuclear spin polarization on pyruvate using parahydrogen, paving the way for applications in biophysical studies on proteins in vitro, on metabolism in cell cultures, or on disease states *in vivo*.

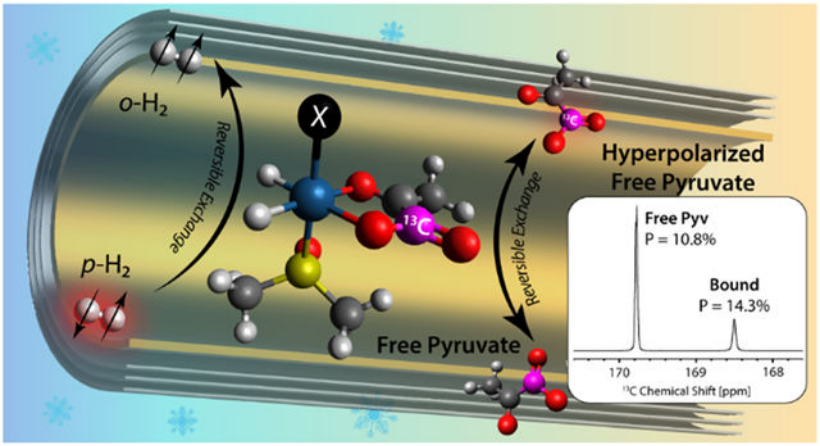

Introduction

Hyperpolarized magnetic resonance imaging (MRI) is emerging as a technique to track biomolecular metabolism without radioactive labels or ionizing radiation.[1] Hyperpolarized (HP) MRI is currently under investigation in clinical trials to gain insights and diagnose metabolic disease states such as cancer[1], diabetes[2], or cardiovascular disease[3,4]. HP pyruvate is as a leading candidate as metabolic marker due to its safety and its central role in metabolism.[1] Through measuring pyruvate metabolism, striking advancements have been made in the detection of cancer cells in prostate[5,6], breast[7], and brain[8] tissues[9]. However, the leading method to hyperpolarize pyruvate, dissolution dynamic nuclear polarization (d-DNP), is limited in broad availability due to its high cost (≈$2.5M), long contrast agent production times (≈30 min or more), and instrument complexity.[10,11] In contrast, Signal Amplification By Reversible Exchange (SABRE)[12] is a fast (≈20 s), cheap (≈$25k), and scalable hyperpolarization technique using parahydrogen (p-H_2) as a source of spin order to directly hyperpolarize small molecules in solutions, including pyruvate.[12-15]

The hyperpolarization of heteronuclei (*e.g.*, ^{13}C) is optimized in magnetic shields that establish μT magnetic fields, called SABRE in Shield Enables Alignment Transfer to Heteronuclei (SABRE-SHEATH).[16-18] Previous work has demonstrated ^{13}C pyruvate hyperpolarization with SABRE-SHEATH, but remained limited in polarization relative to the high values of DNP (1.7% vs. ≈60%).[13,14] Here, we present a combination of advances including the use of temperature cycling to overcome the *in vivo* polarization threshold of 10% with SABRE-SHEATH. The results of this study also indicate that further optimization is possible to maximize the critical molar polarization, defined as the product of concentration and polarization (introduced by Shchepin et al.[19] and Knecht et al.[20]), ultimately the most important hyperpolarization parameter required for *in vivo* translation.[5,11,21]

Previous demonstrations of parahydrogen induced polarization with side arm hydrogenation (PHIP-SAH) on pyruvate have shown the feasibility of *in vivo* studies.[22,23] These experiments demonstrate that an initial ^{13}C polarization of 10%, which was purified to give a 35 mM 3.5% polarization solution at the time of injection, is sufficient for *in vivo* chemical-shift MRI.[22] PHIP-SAH involves synthesis of a propargyl pyruvate precursor, hydrogenation, complex spin transfer, hydrolysis, and phase transfer steps to obtain HP pyruvate.[22] In contrast, the facile nature of SABRE enables direct hyperpolarization of the ^{13}C spins in pyruvate with reduced complexity. Figure 1 highlights the catalytically active species originally described by Iali *et al.*, where optimized hyperpolarization levels of [1-^{13}C]-pyruvate reached 0.96%,[13] substantially below the ^{13}C polarization achieved with DNP[6] or the PHIP-SAH methods.[22,24]

In the present work, we highlight that sufficiently fast *p*-H_2 exchange still occurs in the complex at low temperatures to efficiently polarize bound pyruvate. Using this feature, we implement time-dependent temperature gradients with SABRE-SHEATH on [1-^{13}C]-pyruvate to reach P_{13C} (^{13}C polarization) 10.8% on free pyruvate in solution, which is over six times greater than previous optimized results (Figure 2A). Additionally, this figure is on par with the initial polarization achieved on allyl pyruvate with SAH-PHIP,[22] indicating that with simple purification methods[20,24] a viable biocompatible injectable for *in vivo* imaging could be produced. This is enabled by starting with P_{13C} ≈20% on catalyst-bound pyruvate at lower temperatures. We also provide detailed insights and a kinetic model to describe exchange dynamics and relaxation processes during temperature gradients, which modulate substrate and hydride exchange rates. As detailed below, further optimization yields even greater molar polarization levels (conc. × %*P*) as needed for *in vivo* studies.[9,20,22]

Results and Discussion

The spectrum and results shown in Figure 2A are the maximum achieved single-shot polarization. This data shows 14.3% polarization on bound pyruvate (after warm-up), and 10.8% on the free pyruvate, corresponding to a total polarization of 11.8%. The calculation of %*P* uses the reference signal displayed in Fig. 2B, and is detailed in the SI. This result is enabled by, a) the use of high catalyst to substrate ratio (5 eqv. pyruvate, 3.3 eqv. DMSO), as done in previous work,[14,25] b) the use of [1-^{13}C]-pyruvate, (both [2-^{13}C]-pyruvate and [1,2-$^{13}C_2$]-pyruvate give lower polarization under identical conditions), and c) pre-cooling

to slow exchange followed by bubbling at elevated temperature causing a time-dependent temperature gradient. To ensure reproducibility, we conducted the same experiment five times on different days and obtained an average of 10±1% polarization on free pyruvate (see SI section 8). On bound pyruvate, polarization levels approaching 20% are observed when bubbling at even lower temperatures as detailed below.

Using the high polarization on [1-^{13}C]pyruvate, we acquired a ^{13}C image, shown in Figure 2C, utilizing a fast spin echo sequence at 1.5 T of a cryogen-free MRI system that can be operated at any field between 5 mT and 3 T. At the clinically relevant field of 1.5 T, we imaged the sample directly in an NMR tube with sub-mm resolution. The HP signal enables 3D multi-slice ^{13}C-imaging of the 3.45 mm cross-sectional area of the NMR tube (full details are provided in the SI). As can be seen in the images, even the small, sub mm sized capillary can be resolved in the images.

To characterize the temperature dependence of the hyperpolarization, we conducted the experiments depicted in Figures 3A-E. We used a pneumatic shuttle,[26] where the sample is first cooled in the probe and subsequently shuttled out of the cooled atmosphere into magnetic shields for SABRE-SHEATH[13,27,28]. Figure 3E shows the change in sample temperature as a function of bubbling time when starting at a sample temperature of 0 °C. The temperature was assessed with the internal methanol thermometer (see SI).

At low initial temperature, the slower exchange promotes efficient polarization buildup on the catalyst-bound pyruvate. This effect is evidenced by up to 20% polarization on the catalyst-bound pyruvate achieved by starting at the lowest temperature of −10 °C (see Figure 3C). With only 15 s of bubbling (Figure 3B) the polarization remains almost exclusively on the bound species **3b**. In contrast to previous work,[14] our data suggests that at low temperatures, efficient hydrogen exchange still occurs on **3b** and **3a** species yet at a sufficiently slow rate to allow the weak hydride-^{13}C couplings to pump large degrees of polarization onto bound ^{13}C pyruvate, which barely exchanges. As the sample warms during the bubbling period, [1-^{13}C]-pyruvate can exchange off the catalyst more rapidly while SABRE continues, albeit with reduced efficiency, ultimately leading to high polarization on free pyruvate. As is evident from Figure 3B and 3C, at even further elevated temperatures the free and bound polarization numbers equilibrate due to efficiently exchanging polarization pools. To unequivocally confirm that experiments with a temperature gradient give higher polarization than experiments with constant temperature, we conducted the study shown in Figure 3F. For this direct comparison, we had to use manual sample transfer experiments with a 1.1 T benchtop NMR spectrometer. In these experiments, the sample is either bubbled in a water bath at constant temperature in a magnetic shield (purple, Figure 3F) or first pre-cooled in a water bath at a set temperature and then bubbled in the shield at ambient temperature (green, Figure 3F). The constant temperature experiments consistently stay below the experiments with temperature gradients —lower relative polarization values in this data, compared to automated shuttling, are due to unavoidable inconsistencies in slow manual sample transfer. Additionally, the temperature gradient experienced in this setup is different than in shuttling. In the shuttling system, the sample is bubbled in an atmosphere of ≈14 °C (see Figure 3E), while in the manual transfer experiments the sample is just moved into a room temperature (≈23°C) atmosphere.

Relaxation and polarization build-up data shown in Figure 4 additionally support and characterize the described dynamics. We fit the data to a two-state (bound - free) model, which we developed inspired by previous work.[29] First, for relaxation dynamics in the absence of a pumping term (Figure 4 A), the model takes into account chemical exchange and relaxation of the bound and free pyruvate species.

$$\frac{dP_B}{dt} = -(k+\rho_B)\,P_B[t] + k \cdot P_F[t] \tag{1}$$

$$\frac{dP_F}{dt} = k \cdot P_B[t] - (k+\rho_F)\,P_F[t] \tag{2}$$

Here p_B and p_F are the free and bound polarization, k is the pyruvate exchange rate, and ρ_B and ρ_F are the relaxation rates of the free and bound pyruvates species. Solving the system of differential equations yields a fitting function for the bound and free spin relaxation. The full derivation of the fitting functions is given in the SI.

After solving these differential equations, we use the resulting model to fit the relaxation data in Figure 4A. At t=0 the bound polarization exceeds the free polarization. The difference of the two is illustrated by the purple curve in Figure 4A. Initially, bound polarization decreases quickly because of exchange and relaxation. In contrast, the free polarization only experiences very slow initial decrease because of the exchange with the highly polarized bound species. After about 8 s, the free polarization surpasses the bound polarization due to faster relaxation of the bound species.

A similar model is used to fit the polarization build-up data displayed in Fig. 4B. The only difference is that we introduce a temperature (i.e. bubbling-time) dependent polarization pumping rate, $\boldsymbol{\Gamma}$.

$$\frac{dP_B}{dt} = \boldsymbol{\Gamma} - (k+\rho_B)\,P_B[t] + k \cdot P_F[t] \tag{3}$$

$$\frac{dP_F}{dt} = k \cdot P_B[t] - (k+\rho_F)\,P_F[t] \tag{4}$$

$$\boldsymbol{\Gamma} = b + a \cdot e^{-\frac{t}{\tau}} \tag{5}$$

where Eq. 4 is identical to Eq. 2. The present model for Γ is purely empirical with fit parameters b, a, and τ. After solving this new set of differential equations, only k, b, a, and τ are used as fit parameters. ρ_B and ρ_F are used as extracted from the relaxation data (see SI for details). With this model, the fits explain the rapid initial build-up of bound polarization where pumping is efficient, yet pyruvate exchange is inefficient. We point out that without a temperature-dependent pumping rate Γ, the resulting models cannot represent the data in any reasonable way even if a temperature-dependent k is used. It appears that

Γ has a larger temperature dependence than the pyruvate exchange k. In forthcoming work, we will examine this question and characterize the activation parameters of both hydrogen and pyruvate exchange in full. In the current absence of activation enthalpy and entropy and without knowledge of the exact J-coupling values that drive polarization transfer from p-H_2 to bound [1-^{13}C]-pyruvate, the empirical model for Γ gives valuable information, showing that hydrogen exchange becomes too fast at elevated temperatures to effectively drive SABRE. Therefore, temperature cycling solves the conundrum of having to optimize both hydrogen and substrate exchange simultaneously.

Finally, in Figure 4C we illustrate that p-H_2 is not the limiting substrate at pressures above 75 psi for the investigated sample composition of 6 mM Ir-IMes catalyst, 20 mM DMSO and 30 mM [1-^{13}C]-pyruvate. This graph implies that at higher substrate and catalyst concentrations the p-H_2 pressure can be increased to maintain the same polarization levels while boosting the ultimately important molar polarization. This insight is further stressed by the results displayed in Figure 4D, which demonstrate the scalability of ^{13}C pyruvate polarization from 30 mM [1-^{13}C]-pyruvate (where all the previously discussed results were obtained) to 60 mM [1-^{13}C]-pyruvate (maintaining the same ratios of catalyst and DMSO). Doubling of the concentration actually leads to an increase in polarization, more than doubling the molar polarization, indicating that 60 mM [1-^{13}C]-pyruvate may be the ideal concentration for future studies. Shifting to an even higher concentration yielded slightly reduced polarization, however these higher concentrated samples are likely to be parahydrogen limited (see Figure 4C), so higher p-H_2 pressures may return similar polarization levels, while boosting molar polarization.

Conclusion

In summary, we demonstrated a high (11.8% weighted average) total polarization for [1-^{13}C]-pyruvate and 10.8% free polarization paving the way for further optimization and significantly enhancing the feasibility of *in vivo* work. Specifically, the facile and robust nature of SABRE hyperpolarization relative to other hyperpolarization methods make it an easily scalable technology. In these results, we emphasize the role that spin system, sample composition, and temperature gradients play in achieving high polarization levels. A kinetic model of differential equations was used to rationalize the high polarization levels. We used these high polarization levels to acquire multi-slice HP ^{13}C images with a cryogen-free MRI system operated at 1.5 T. This achievement indicates that it is possible to combine low-cost hyperpolarization with low-cost MRI to achieve high-sensitivity molecular imaging. Future work will focus on partnering these methods with previous demonstrations of catalyst extraction[30] or phase-switching[31] to achieve safely injectable solutions for *in vivo* demonstrations at the preclinical level, driving this technology toward clinical applications.

Supplementary Material

Refer to Web version on PubMed Central for supplementary material.

ACKNOWLEDGMENT

Research reported in this publication was supported by the National Institute of Biomedical Imaging and Bioengineering of the National Institutes of Health under Award Numbers NIH R21EB025313 and NIH R01EB029829. The content is solely the responsibility of the authors and does not necessarily represent the official views of the National Institutes of Health. In addition, we acknowledge funding from the Mallinckrodt Foundation, the National Science Foundation under award NSF CHE-1904780, and from the National Cancer Institute under award number NCI 1R21CA220137, as well as funding from the North Carolina Biotechnology Center in the form of a Translational Research Grant. Finally, we would like to acknowledge the support from NCSU's METRIC providing access to NMR instrumentation.

REFERENCES

(1). Serrao EM; Brindle KM Potential Clinical Roles for Metabolic Imaging with Hyperpolarized [1-13C]Pyruvate. Front. Oncol 2016, 6 (MAR), 1–6. [PubMed: 26858933]

(2). Rider OJ; Apps A; Miller JJJJ; Lau JYC; Lewis AJM; Peterzan MA; Dodd MS; Lau AZ; Trumper C; Gallagher FA; Grist JT; Brindle KM; Neubauer S; Tyler DJ Noninvasive in Vivo Assessment of Cardiac Metabolism in the Healthy and Diabetic Human Heart Using Hyperpolarized 13C MRI. Circ. Res. 2020, 126, 725–736. [PubMed: 32078413]

(3). Cunningham CH; Lau JYC; Chen AP; Geraghty BJ; Perks WJ; Roifman I; Wright GA; Connelly KA Hyperpolarized 13C Metabolic MRI of the Human Heart: Initial Experience. Circ. Res 2016, 119 (11), 1177–1182. [PubMed: 27635086]

(4). Lewis AJM; Tyler DJ; Rider O Clinical Cardiovascular Applications of Hyperpolarized Magnetic Resonance. Cardiovasc. Drugs Ther 2020, 34 (2), 231–240. [PubMed: 32020468]

(5). Shukla-Dave A; Hricak H Role of MRI in Prostate Cancer Detection. NMR Biomed. 2014, 27 (1), 16–24. [PubMed: 23495081]

(6). Nelson SJ; Kurhanewicz J; Vigneron DB; Larson PEZ; Harzstark AL; Ferrone M; van Criekinge M; Chang JW; Bok R; Park I; Reed G; Carvajal L; Small EJ; Munster P; Weinberg VK; Ardenkjaer-Larsen JH; Chen AP; Hurd RE; Odegardstuen L-I; Robb FJ; Tropp J; Murray JA Metabolic Imaging of Patients with Prostate Cancer Using Hyperpolarized [1-13C]Pyruvate. Sci. Transl. Med 2013, 5 (198), 198ra108.

(7). Gallagher FA; Woitek R; McLean MA; Gill AB; Garcia RM; Provenzano E; Riemer F; Kaggie J; Chhabra A; Ursprung S; Grist JT; Daniels CJ; Zaccagna F; Laurent MC; Locke M; Hilborne S; Frary A; Torheim T; Boursnell C; Schiller A; Patterson I; Slough R; Carmo B; Kane J; Biggs H; Harrison E; Deen SS; Patterson A; Lanz T; Kingsbury Z; Ross M; Basu B; Baird R; Lomas DJ; Sala E; Wason J; Rueda OM; Chin SF; Wilkinson IB; Graves MJ; Abraham JE; Gilbert FJ; Caldas C; Brindle KM Imaging Breast Cancer Using Hyperpolarized Carbon-13 MRI. Proc. Natl. Acad. Sci. U. S. A 2020, 117 (4), 2092–2098. [PubMed: 31964840]

(8). Miloushev VZ; Granlund KL; Boltyanskiy R; Lyashchenko SK; DeAngelis LM; Mellinghoff IK; Brennan CW; Tabar V; Yang TJ; Holodny AI; Sosa RE; Guo YWW; Chen AP; Tropp J; Robb F; Keshari KR Metabolic Imaging of the Human Brain with Hyperpolarized 13C Pyruvate Demonstrates 13C Lactate Production in Brain Tumor Patients. Cancer Res. 2018, 78 (14), 3755–3760. [PubMed: 29769199]

(9). Vaeggemose M; Schulte RF; Laustsen C Comprehensive Literature Review of Hyperpolarized Carbon-13 Mri: The Road to Clinical Application. Metabolites 2021, 11 (4), 219. [PubMed: 33916803]

(10). Ardenkjaer-Larsen JH; Boebinger GS; Comment A; Duckett S; Edison AS; Engelke F; Griesinger C; Griffin RG; Hilty C; Maeda H; Parigi G; Prisner T; Ravera E; Van Bentum J; Vega S; Webb A; Luchinat C; Schwalbe H; Frydman L Facing and Overcoming Sensitivity Challenges in Biomolecular NMR Spectroscopy. Angew. Chemie - Int. Ed 2015, 54 (32), 9162–9185.

(11). Nikolaou P; Goodson BM; Chekmenev EY NMR Hyperpolarization Techniques for Biomedicine. Chem. - A Eur. J 2015, 21 (8), 3156–3166.

(12). Adams RW; Aguilar JA; Atkinson KD; Cowley MJ; Elliott PIPP; Duckett SB; Green GGRR; Khazal IG; Lopez-Serrano J; Williamson DC Reversible Interactions with Para-Hydrogen Enhance NMR Sensitivity by Polarization Transfer. Science (80-.). 2009, 323 (5922), 1708–1711.

(13). Iali W; Roy SS; Tickner BJ; Ahwal F; Kennerley AJ; Duckett SB Hyperpolarising Pyruvate through Signal Amplification by Reversible Exchange (SABRE). Angew. Chemie 2019, 131 (30), 10377–10381.

(14). Tickner BJ; Semenova O; Iali W; Rayner PJ; Whitwood AC; Duckett SB Optimisation of Pyruvate Hyperpolarisation Using SABRE by Tuning the Active Magnetisation Transfer Catalyst. Catal. Sci. Technol 2020, 10 (5), 1343–1355. [PubMed: 32647563]

(15). Barskiy DA; Knecht S; Yurkovskaya AV; Ivanov KL SABRE: Chemical Kinetics and Spin Dynamics of the Formation of Hyperpolarization. Prog. Nucl. Magn. Reson. Spectrosc 2019, 114–115, 33–70.

(16). Barskiy DA; Shchepin RV; Tanner CPN; Colell JFP; Goodson BM; Theis T; Warren WS; Chekmenev EY The Absence of Quadrupolar Nuclei Facilitates Efficient13C Hyperpolarization via Reversible Exchange with Parahydrogen. ChemPhysChem 2017, 18 (12), 1493–1498. [PubMed: 28517362]

(17). Truong ML; Theis T; Coffey AM; Shchepin RV; Waddell KW; Shi F; Goodson BM; Warren WS; Chekmenev EY ^{15}N Hyperpolarization by Reversible Exchange Using SABRE-SHEATH. J. Phys. Chem. C 2015, 119 (16), 8786–8797.

(18). Theis T; Truong ML; Coffey AM; Shchepin RV; Waddell KW; Shi F; Goodson BM; Warren WS; Chekmenev EY Microtesla SABRE Enables 10% Nitrogen-15 Nuclear Spin Polarization. J. Am. Chem. Soc 2015, 137 (4), 1404–1407. [PubMed: 25583142]

(19). Shchepin RV; Birchall JR; Chukanov NV; Kovtunov KV; Koptyug IV; Theis T; Warren WS; Gelovani JG; Goodson BM; Shokouhi S; Rosen MS; Yen Y; Pham W; Chekmenev EY Hyperpolarizing Concentrated Metronidazole 15 NO 2 Group over Six Chemical Bonds with More than 15 % Polarization and a 20 Minute Lifetime. Chem. – A Eur. J 2019, 25 (37), 8829–8836.

(20). Knecht S; Blanchard JW; Barskiy D; Cavallari E; Dagys L; van Dyke E; Tsukanov M; Bliemel B; Münnemann K; Aime S; Reineri F; Levitt MH; Buntkowsky G; Pines A; Blümler P; Budker D; Eills J Rapid Hyperpolarization and Purification of the Metabolite Fumarate in Aqueous Solution. Proc. Natl. Acad. Sci. U. S. A 2021, 118 (13), 1–6.

(21). Kovtunov KV; Pokochueva EV; Salnikov OG; Cousin SF; Kurzbach D; Vuichoud B; Jannin S; Chekmenev EY; Goodson BM; Barskiy DA; Koptyug IV Hyperpolarized NMR Spectroscopy: D-DNP, PHIP, and SABRE Techniques. Chem. - An Asian J 2018, 13 (15), 1857–1871.

(22). Cavallari E; Carrera C; Sorge M; Bonne G; Muchir A; Aime S; Reineri F The 13C Hyperpolarized Pyruvate Generated by ParaHydrogen Detects the Response of the Heart to Altered Metabolism in Real Time. Sci. Rep 2018, 8 (1), 8366. [PubMed: 29849091]

(23). Cavallari E; Carrera C; Aime S; Reineri F 13C MR Hyperpolarization of Lactate by Using ParaHydrogen and Metabolic Transformation in Vitro. Chem. - A Eur. J 2017, 23 (5), 1200–1204.

(24). Cavallari E; Carrera C; Aime S; Reineri F Studies to Enhance the Hyperpolarization Level in PHIP-SAH-Produced C13-Pyruvate. J. Magn. Reson 2018, 289, 12–17. [PubMed: 29448129]

(25). Chapman B; Joalland B; Meersman C; Ettedgui J; Swenson RE; Krishna MC; Nikolaou P; Kovtunov KV; Salnikov OG; Koptyug IV; Gemeinhardt ME; Goodson BM; Shchepin RV; Chekmenev EY Low-Cost High-Pressure Clinical-Scale 50% Parahydrogen Generator Using Liquid Nitrogen at 77 K. Anal. Chem 2021, 93 (24), 8476–8483. [PubMed: 34102835]

(26). TomHon P; Akeroyd E; Lehmkuhl S; Chekmenev EY; Theis T Automated Pneumatic Shuttle for Magnetic Field Cycling and Parahydrogen Hyperpolarized Multidimensional NMR. J. Magn. Reson 2020, 312, 106700. [PubMed: 32092678]

(27). Theis T; Truong ML; Coffey AM; Shchepin RV; Waddell KW; Shi F; Goodson BM; Warren WS; Chekmenev EY Microtesla SABRE Enables 10% Nitrogen-15 Nuclear Spin Polarization. J. Am. Chem. Soc 2015, 137 (4), 1404–1407. [PubMed: 25583142]

(28). Colell JFP; Logan AWJ; Zhou Z; Shchepin R; Barskiy DA; Ortiz GX; Wang Q; Malcolmson SJ; Chekmenev EY; Warren WS; Theis T Generalizing, Extending, and Maximizing Nitrogen-15 Hyperpolarization Induced by Parahydrogen in Reversible Exchange. J. Phys. Chem. C 2017, 121 (12), 6626–6634.

(29). Hermkens NKJ; Feiters MC; Rutjes FPJT; Wijmenga SS; Tessari M High Field Hyperpolarization-EXSY Experiment for Fast Determination of Dissociation Rates in SABRE Complexes. J. Magn. Reson 2017, 276 (2017), 122–127.

(30). Kidd BE; Gesiorski JL; Gemeinhardt ME; Shchepin RV; Kovtunov KV; Koptyug IV; Chekmenev EY; Goodson BM Facile Removal of Homogeneous SABRE Catalysts for Purifying Hyperpolarized Metronidazole, a Potential Hypoxia Sensor. J. Phys. Chem. C 2018, 122 (29), 16848–16852.

(31). Iali W; Olaru AM; Green GGR; Duckett SB Achieving High Levels of NMR-Hyperpolarization in Aqueous Media With Minimal Catalyst Contamination Using SABRE. Chem. - A Eur. J 2017, 23 (44), 10491–10495.

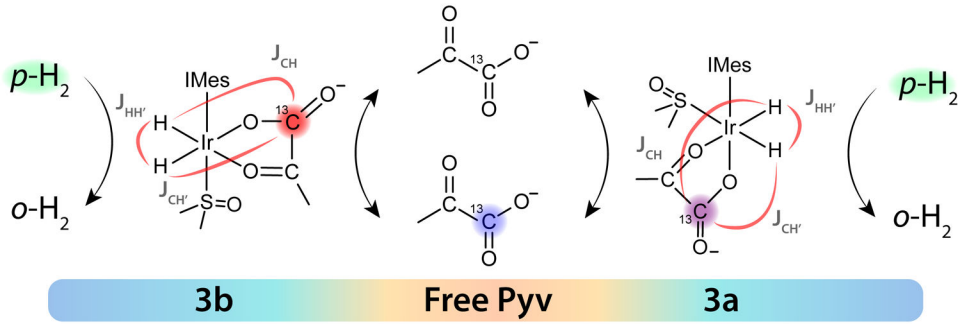

Figure 1.

Hyperpolarization scheme of [1-^{13}C]-pyruvate, with a gradient representation of temperature cycling. The full IMes ligand is omitted for diagram clarity, where IMes = 1,3 - bis(2,4,6 - trimethylphenyl) imidazole-2-ylidene.

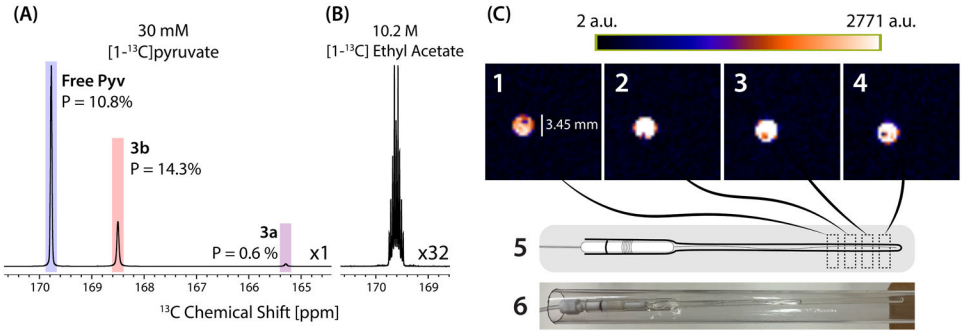

Figure 2.

(A) NMR spectrum of hyperpolarized [1-^{13}C]-pyruvate in free and catalyst-bound forms. This spectrum was acquired with a sample of 30 mM [1-^{13}C]-pyruvate, 20 mM DMSO, and 6 mM IMes catalyst in CD_3OD. (B) Thermal reference spectrum of [1-^{13}C]-ethyl acetate at 9.4 T, used for calculation of the polarization. (C) MRI of HP [1-^{13}C]-pyruvate sample of 60 mM [1-^{13}C]-pyruvate, 40 mM DMSO, and 12 mM IMes catalyst in CH_3OH. Four axial slices of the image are taken in 1-4, with the NMR tube phantom and corresponding slice positioning shown in 5 and 6. The images are acquired with a fast spin echo sequence at 1.5 T with 64×64 voxels, 30×30 mm^2 FOV, a single echo train with 64 lines, and an overall acquisition time of 1.5 s. Full details regarding the setup and sequence are in the SI. The polarization obtained in the MRI was 5.85% by comparison to a thermal phantom.

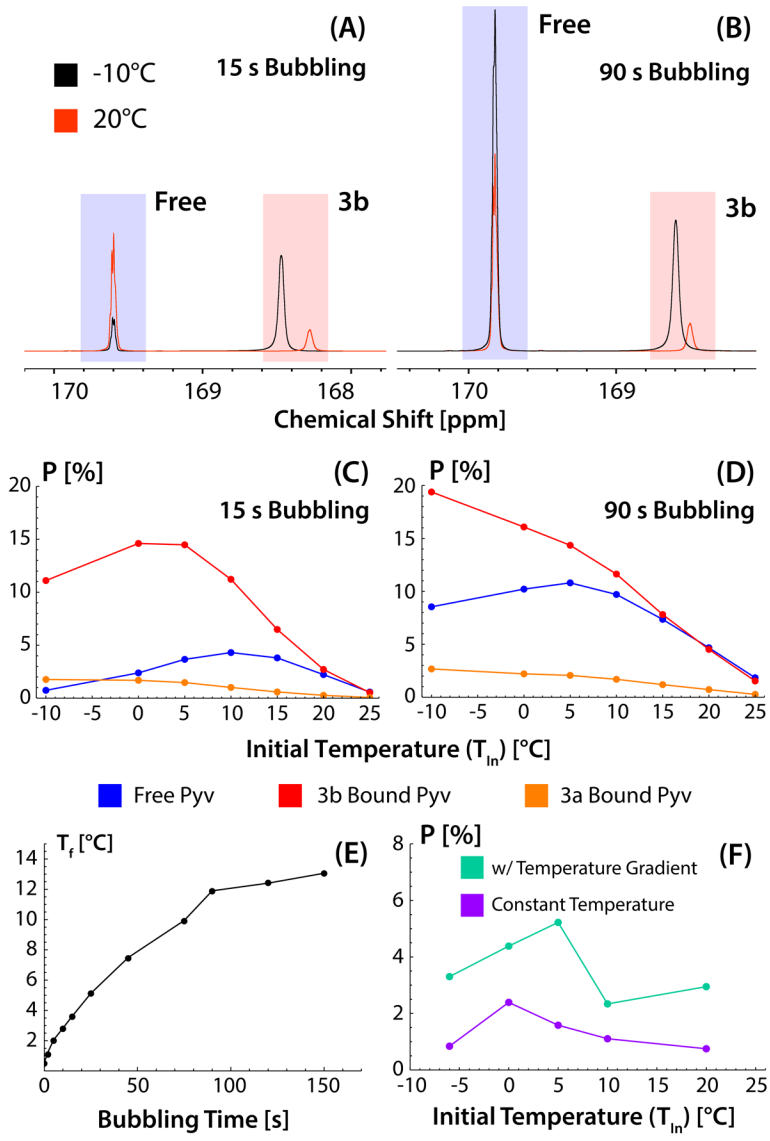

Figure 3.

Variable temperature comparisons in the hyperpolarization of [1-^{13}C]-pyruvate. (A,B) Comparison of HP spectra obtained with an initial sample temperature of −10°C and 20°C using (A) 15 s bubbling and (B) 90 s bubbling. (C,D) Comparison of the temperature dependence of [1-^{13}C]-pyruvate hyperpolarization with (C) 15 s bubbling and (D) 90 s bubbling. (E) Final sample temperature with variable bubbling time for an initial sample temperature of 0°C in the pneumatic shuttling setup. (F) Comparison of polarization obtained on free pyruvate with and without a temperature gradient using manual sample transfer.

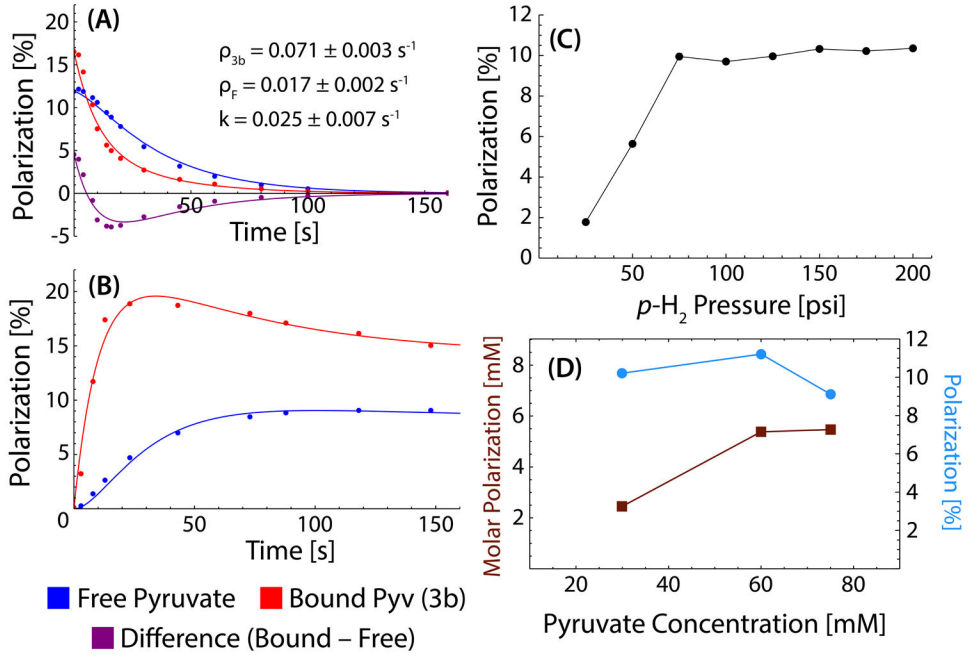

Figure 4.

Relaxation, build-up, pressure, and concentration dependence. (A) Low-field (0.3 μT) relaxation and (B) polarization build-up data for free and bound pyruvate. Relaxation data is acquired after p-H_2 bubbling is stopped followed by a variable delay, while buildup data is acquired with variable bubbling periods. The data are fit to curves derived from the discussed differential equations (Eq. 1-5). Since the resulting analytical solutions are lengthy, they are integrated and detailed in the SI. Table 5 in the SI gives all fit parameters. In A the temperature is constant and approx. 14 °C. (C) Pressure dependence of pyruvate polarization. (D) Sample concentration dependence for pyruvate polarization and molar polarization. Catalyst and DMSO concentrations are scaled at constant ratio. All data are acquired using an initial sample temperature of 0 °C.